Acta Pharmaceutica Sinica B 2023;13(2):722−738

Chinese Pharmaceutical Association
Institute of Materia Medica, Chinese Academy of Medical Sciences

Acta Pharmaceutica Sinica B

www.elsevier.com/locate/apsb
www.sciencedirect.com

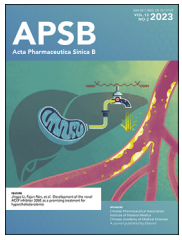

ORIGINAL ARTICLE

A novel and low-toxic peptide DR3penA alleviates pulmonary fibrosis by regulating the MAPK/miR-23b-5p/AQP5 signaling axis

Dan Wang[a,b], Bochuan Deng[a,b], Lu Cheng[a,b], Jieru Li[a,b], Jiao Zhang[a,b], Xiang Zhang[a,b], Xiaomin Guo[a,b], Tiantian Yan[a,b], Xin Yue[a,b], Yingying An[a,b], Bangzhi Zhang[a,b], Wenle Yang[a,b], Junqiu Xie[a,b,*], Rui Wang[a,b,*]

[a]*Institute of Materia Medica and Research Unit of Peptide Science, Chinese Academy of Medical Sciences, Peking Union Medical College, Beijing 100050, China*
[b]*Key Laboratory of Preclinical Study for New Drugs of Gansu Province, School of Basic Medical Sciences, Lanzhou University, Lanzhou 730000, China*

Received 24 April 2022; received in revised form 19 August 2022; accepted 25 August 2022

KEY WORDS

Peptide;
Structure modification;
Pulmonary fibrosis;
miR-23b-5p;
AQP5

Abstract Pulmonary fibrosis (PF) is a pathological change caused by repeated injuries and repair dysfunction of the alveolar epithelium. Our previous study revealed that the residues Asn3 and Asn4 of peptide DR8 (DHNNPQIR-NH_2) could be modified to improve stability and antifibrotic activity, and the unnatural hydrophobic amino acids α-(4-pentenyl)-Ala and D-Ala were considered in this study. DR3penA (DHα-(4-pentenyl)-ANPQIR-NH_2) was verified to have a longer half-life in serum and to significantly inhibit oxidative damage, epithelial−mesenchymal transition (EMT) and fibrogenesis *in vitro* and *in vivo*. Moreover, DR3penA has a dosage advantage over pirfenidone through the conversion of drug bioavailability under different routes of administration. A mechanistic study revealed that DR3penA increased the expression of aquaporin 5 (AQP5) by inhibiting the upregulation of miR-23b-5p and the mitogen-activated protein kinase (MAPK) pathway, indicating that DR3penA may alleviate PF by regulating MAPK/miR-23b-5p/AQP5. Safety evaluation showed that DR3penA is a peptide drug without obvious toxicity or acute side effects and has significantly improved safety compared to DR8. Thus, our findings suggest that DR3penA, as a novel and low-toxic peptide, has the potential to be a leading

*Corresponding authors. Tel.: +86 931 8915522; fax: +86 931 8911255.
E-mail addresses: xiejq@lzu.edu.cn (Junqiu Xie), wangrui@lzu.edu.cn (Rui Wang).

Peer review under responsibility of Chinese Pharmaceutical Association and Institute of Materia Medica, Chinese Academy of Medical Sciences.

https://doi.org/10.1016/j.apsb.2022.09.001

compound for PF therapy, which provides a foundation for the development of peptide drugs for fibrosis-related diseases.

1. Introduction

Pulmonary fibrosis (PF) is a pathological change in the development of a variety of chronic lung diseases to the end stage, which leads to the destruction of lung structure and function, respiratory failure and ultimately death. Although pirfenidone and nintedanib were demonstrated to delay the progression of PF in the clinic, the disadvantages of side effects, high costs and failure to reverse disease cannot be ignored[1,2]. Therefore, it is of great significance to find drugs with stable therapeutic effects, few side effects and high safety for PF treatment.

The pathological feature of PF is abnormal communication between epithelial cells and fibroblasts triggered by repeated microinjury of alveolar epithelial cells, which promotes extracellular matrix (ECM) deposition and pathological remodeling of lung tissue[3]. Lung myofibroblasts derived from epithelial−mesenchymal transition (EMT), resident fibroblasts and circulating fibrocytes can regulate the expression and secretion of ECM components, while the ECM further promotes the activation of fibroblasts[4]. The formed positive feedback loop contributes to accelerating the progression of PF. Moreover, ROS produced by inflammatory cells, fibroblasts and myofibroblasts after lung injury participate in epithelial cell apoptosis, fibroblast differentiation and ECM accumulation[5−7]. A high level of oxidative stress in patients with idiopathic pulmonary fibrosis is significantly correlated with pulmonary function indices (FVC and DLCO) and the severity of dyspnea (MRC score)[8]. Therefore, ECM deposition, EMT and ROS generation are crucial for the pathogenesis and development of PF.

microRNAs (miRNAs) are endogenous single stranded non-coding RNAs of approximately 22 nucleotides that bind to the 3′UTR of target mRNAs to regulate posttranscriptional level, thus affecting cell processes[9,10]. miRNAs participate in the progression of PF by regulating lung epithelial repair, EMT, the proliferation and differentiation of fibroblasts, ECM deposition and oxidative stress[11]. Studies have shown that miR-200, miR-34, miR-182 and let-7d are involved in EMT and that miR-9-5p is correlated with redox regulation in PF[11−13]. miR-23b-5p plays critical roles in the progression of several diseases, such as cancer, acute myeloid leukemia, and cardiac hypertrophy and dysfunction[14−17]. In this study, according to transcriptome sequencing analysis, miR-23b-5p was found to be differentially expressed in mice in the normal control and PF model groups, suggesting that miR-23b-5p contributes to the progression of PF.

Aquaporin 5 (AQP5) is mainly expressed in airway and alveolar epithelial cells. Abnormal expression of AQP5 causes a variety of respiratory diseases, such as lung injury, inflammation, fibrosis, chronic obstructive pulmonary disease, asthma and cancer[18−23]. AQP5 can promote the clearance of alveolar fluid and maintain the integrity of alveolar epithelial cells, which is essential for gas exchange and the regulation of lung water content. Therefore, the epithelial cell injury decreases the level of AQP5, and downregulation of AQP5 further promotes lung injury caused by destruction of the epithelial barrier[24].

Peptide drugs have the advantages of higher bioactivity, selectivity, permeability, target potency and safety compared with small-molecule and protein drugs[25]. Therefore, peptides have been widely used in the treatment of cancer, diabetes, acquired immunodeficiency syndrome and cardiovascular diseases[26−29]. Our previous studies revealed that the antioxidant peptide DR8 (DHNNPQIR-NH_2) derived from rapeseed protein showed low toxicity and an inhibitory effect on organ fibrosis, such as lung, kidney and liver fibrosis[30−32]. However, as a natural peptide, DR8 exhibited poor stability and a high effective concentration in cells. A structure−activity relationship study revealed that the anti-fibrotic activity and serum stability were improved after Asn3, Asn4, Ile7 and Arg8 of DR8 were substituted with D-amino acids or alanine[33]. In the current study, DR8 was further designed and modified based on previous results. A series of DR8 analogs were synthetized and screened, from which analog DR3penA (DHα-(4-pentenyl)-ANPQIR-NH_2) was found to be a peptide with potential antifibrotic activity. Therefore, the stability, anti-pulmonary fibrotic effect, mechanism and safety of the peptide DR3penA were further explored in this study.

2. Materials and methods

2.1. Peptide synthesis

All peptides were synthesized using the Fmoc-based solid-phase peptide synthesis method, and the crude peptides were separated and purified *via* reverse-phase HPLC (RP-HPLC, Waters, Milford, USA). The peptide sequences were confirmed by mass spectrometry (Supporting Information Fig. S12). RP-HPLC was used to analyze the purity, and the peptides with a purity over 95% were used for the following experiments (Supporting Information Fig. S13).

2.2. Serum stability assay

The blood of C57BL/6 mice was collected and the supernatant was used for stability detection after centrifugation. Peptides at a concentration of 10 mmol/L were incubated with serum at 37 °C. Samples were taken from the mixture at 0, 15, 30, 60, 120 and 240 min, and then incubated with ice-cold acetonitrile for 10 min. The supernatant was collected after centrifugation. Samples were analyzed *via* RP-HPLC. The formula for calculation of half-life ($t_{1/2}$) was as follows, where A_t is the peak area at t min, A_0 is the peak area at 0 min, K is the elimination rate constant and t is the incubation time.

$$A_t = A_0 e^{-Kt}$$

$$A_t / A_0 = 0.5,\ t_{1/2} = \mathrm{Ln}\,2 / K$$

2.3. Cell culture

NIH3T3 murine embryonic fibroblasts and A549 human lung epithelial cells were maintained in DMEM and RPMI 1640 medium (Gibco, Carlsbad, USA) with 10% FBS (BI, Beit HaEmek, Israel), respectively, at 37 °C with 5% CO_2. In the western blotting, real-time qPCR and immunofluorescence experiments, cells were plated in 6-well plates with complete medium for 24 h. After starvation with serum-free medium overnight, the cells were treated with TGF-β1 (5 ng/mL, PeproTech, Rocky Hill, USA) alone or with various concentrations of peptides. In the studies of the signaling pathway, the inhibitors SP600125, SB203580 and PD98059 (MedChem Express, San Diego, USA) were added to A549 cells at the concentration of 10 μmol/L for 30 min before TGF-β1 and DR3penA treatment. Total RNA and protein were obtained after incubation for 48 h, and phosphorylated protein was extracted after incubation for 1 h.

2.4. Cell migration assay

Cell scratch and migration assays were performed following previously described methods[33]. In this study, A549 cells were treated with DR3penA (2.5 and 10 μmol/L) to study the effect on cell migration.

2.5. Intracellular ROS detection

The intracellular ROS levels in NIH3T3 cells and A549 cells were detected using the fluorescent probe DCFH-DA (Sigma−Aldrich). Cells were plated in glass-bottom cell culture dishes, and TGF-β1 and/or DR3penA (2.5 and 10 μmol/L) were cultured with the cells for 12 h. Then, 10 μmol/L DCFH-DA dissolved in DMSO and diluted with serum-free medium was added to the cell culture dishes. Subsequently, DCFH-DA solution was added to each dish and incubated with the cells for 30 min at 37 °C. The DCFH-DA that failed to enter the cells was washed away with PBS. Images were captured with a confocal laser scanning microscope (Zeiss LSM 710 Meta; Karl, Germany).

2.6. Immunofluorescence

A549 cells were planted in glass-bottom cell culture dishes and treated as previously described. Cells were fixed with 4% paraformaldehyde and blocked with 10% BSA for 15 min and 1 h, respectively. Then, after being washed with PBS, the cells were incubated with the corresponding primary antibody overnight at 4 °C and then with a fluorescent secondary antibody for 2 h to bind the primary antibody. Cell nuclei were stained with DAPI in the absence of light, and images were captured *via* confocal laser scanning microscopy.

2.7. Animals

Female SPF C57BL/6 mice and Kunming mice (of mixed genders) were purchased from Lanzhou Veterinary Research Institute (Lanzhou, China). All animal experiments procedures were carried out according to the Ethics Committee of Lanzhou University (Animal Ethics Approval No. SYXK Gan 2018-0002).

2.8. Models of bleomycin-induced PF and DR3penA treatment

C57BL/6 mice were randomly divided into the following six groups (n = 11 per group): (1) normal control group (normal); (2) saline control group (saline); (3) bleomycin model group (BLM); (4) bleomycin + DR3penA (0.5 mg/kg) group; (5) bleomycin + DR3penA (2.5 mg/kg) group; and (6) bleomycin + pirfenidone (100 mg/kg, PFD) group. After anesthesia, bleomycin (5 mg/kg) was intratracheally injected into mice to establish an animal model of PF, while mice in the saline group received intratracheal injection of the same volume of sterile saline as a control. Mice in the DR3penA group were subcutaneously injected with DR3penA (0.5 or 2.5 mg/kg) daily from Day 1 to Day 21 for preventive treatment. Mice in the pirfenidone group were intragastrically administered pirfenidone (100 mg/kg) and mice in the other groups were administered PBS. The body weight was recorded every other day. Mice were sacrificed on the 22nd day of bleomycin instillation, and blood and lung tissue samples were harvested for the following experiments.

2.9. Acute toxicity assay

Kunming mice were randomly divided into 10 groups (5 female and 5 male mice): (1) PBS control; (2) DR8 (0.5 mg/kg); (3) DR8 (2.5 mg/kg); (4) DR8 (12.5 mg/kg); (5) DR8 (62.5 mg/kg); (6) DR3penA (0.5 mg/kg); (7) DR3penA (2.5 mg/kg); (8) DR3penA (12.5 mg/kg); (9) DR3penA (62.5 mg/kg); and (10) DR3penA (5000 mg/kg). Mice in the DR8 and DR3penA administration groups were injected subcutaneously with peptide at the corresponding dose, while mice in the control group received PBS. The diet, drinking, activity and response to stimulation of mice were observed continually for 6 h after injection of DR8 and DR3penA, and the weight was recorded every other day. After a single administration for 14 days, the mice underwent gross anatomical examination, and then, the organs were photographed, weighed and fixed with 4% formaldehyde for histological assays. Blood was collected, and serum was separated for biochemical analysis.

2.10. Biochemical analysis

The levels of malondialdehyde (MDA), superoxide dismutase (SOD), catalase (CAT), blood urea nitrogen (BUN), serum creatinine (Cr), alanine aminotransferase (ALT) and aspartate aminotransferase (AST) were detected using test kits from Nanjing Jiancheng Bioengineering Institute (Nanjing, China). The procedures were performed following the manufacturers' instructions.

2.11. Histological and immunohistochemical analyses

Tissue samples were fixed with 4% formaldehyde and then embedded in paraffin. The blocks were sectioned at 3−5 μm and placed on a cover glass, which was further used for hematoxylin-eosin (HE) and Masson staining assays after dehydration with gradient ethanol and vitrification with dimethylbenzene. In the immunohistochemical assay, citric acid solution at 0.01 mol/L was used for antigen retrieval after dehydration and vitrification of sections. Subsequently, 4% H_2O_2 was used to block the activity of endogenous peroxidase for 10 min, after which the samples were

blocked with goat serum for 1 h and incubated with the corresponding primary antibody at 4 °C overnight. Then, lung sections were incubated with HRP-conjugated secondary antibody for 15 min to bind with primary antibody (ZSGB-BIO, Beijing, China). Freshly prepared DAB was added to the sections to visualize positive staining. Images were captured using a microscope, and positive staining was analyzed using Image-Pro Plus software.

2.12. *Western blot analysis*

Total protein from the cells or lungs of mice was lysed with RIPA buffer (Beyotime, Shanghai, China) and normalized to 30 μg using 5× loading buffer (Solarbio, Beijing, China) after determining the concentration with a BCA kit (Thermo Fisher Scientific, Rockford, USA). A 10% SDS-PAGE gel was used to separate the proteins which were then transferred onto a PVDF membrane (Millipore, Bedford, USA). The membrane was blocked with 5% nonfat milk or BSA to block nonspecific binding and then immunoblotted with primary antibody at 4 °C overnight. An enhanced chemiluminescence (ECL) kit (Yeasen, Shanghai, China) was used to visualize the protein bands after the membrane was incubated with HRP-conjugated secondary antibody for 1 h. All bands were analyzed using Evolution Capt software, and the expression of target proteins was normalized to that of GAPDH. Relevant information on the antibodies is shown in Supporting Information Table S3.

2.13. *Real-time qPCR analysis*

Total RNA was extracted with TransZol Up (TransGen, Beijing, China) and reverse-transcribed to cDNA with 1st Strand cDNA Synthesis SuperMix for qPCR (Yeason, Shanghai, China) after being quantified by a microspectrophotometer (Kaiao, Beijing, China). The mRNA level of each gene was calculated according to the $2^{-\Delta\Delta Ct}$ method using qPCR SYBR Green Master Mix (Yeason, Shanghai, China). GAPDH was used as a reference gene for mRNA, and U6 was used as a reference gene for miRNA. The sequences of the primer pairs are shown in Supporting Information Table S4.

2.14. *Differential expression analysis and mRNA prediction*

The same parts of lung tissue samples from mice were quickly frozen in liquid nitrogen. Samples were sent to Shanghai Jiejue Gene Technology Co., Ltd. for sequencing. A P-value ≤ 0.05 and $|\text{fold change (FC)}| \geq 1.5$ were set as the screening standards for differentially expressed miRNAs. The target gene of miR-23b-5p was predicted using the miRDB database and TargetScan database.

2.15. *Cell transduction*

A549 cells were transduced with LV-miR-23b and plated in 6-well plates for 24 h. Fresh complete RPMI 1640 medium was used to replace the culture medium containing virus. After 48 h, the cells were observed under a fluorescence microscope to confirm transduction efficiency. More than 80% of the cells showed green fluorescence, indicating successful transduction with LV-miR-23b. Then, 2 μg/mL puromycin was added to the resistance screen. Nonresistant cells were killed, and resistant cells were used for the follow-up experiment.

2.16. *Statistical analysis*

The data are presented as the mean ± SD and represent at least three independent replicates. Statistical analysis was performed using GraphPad Prism 8 software. One-way ANOVA was used to analyze the differences between multiple groups. $P < 0.05$ was considered to indicate statistical significance.

3. Results

3.1. *Activity screening of DR8 analogs and concentration optimizing of peptide DR3penA*

Previous activity screening of peptide DR8 identified that the residues Asn3, Asn4, Ile7 and Arg8 could be modified further to improve anti-fibrotic activity[33]. Moreover, a serum stability assay showed that the half-life was greatly improved after Asn at positions 3 and 4 was substituted by D-Asn, and the antifibrotic activity was obviously improved compared with that of DR8. Therefore, the unnatural hydrophobic amino acids α-(4-pentenyl)-Ala and D-Ala were introduced at positions 3 and 4 of DR8 to improve the stability and antifibrotic activity (Table 1). Cytotoxicity assays indicated that the DR8 analogs including DR3dA, DR4dA, DR3d4dA, DR3penA and DR4penA had no toxicity against NIH3T3 cells at a concentration range of 10−160 μmol/L (Supporting Information Fig. S1A). To evaluate the antifibrotic activity of peptides, the expression of α-SMA, a characteristic protein in myofibroblasts, was measured in TGF-β1-induced NIH3T3 cells after treatment with DR8 analogs at a concentration of 80 μmol/L. The results showed that the analogs DR3penA and DR4penA have better activity in inhibiting the expression of α-SMA protein and a longer half-life than DR8 (Fig. 1A and Table 2). Moreover, compared with DR4penA, DR3penA improved the

Table 1 Sequence, number of amino acids, mass, and retention time of DR8 and its analogs.

Peptide	Sequence[a]	Number of amino acids	Mass (Da)[b]	t_R (min)[c]
DR8	DHNNPQIR-NH_2	8	992.49	6.864
DR3dA	DHANPQIR-NH_2	8	948.49	7.047
DR4dA	DHNAPQIR-NH_2	8	948.49	7.631
DR3d4dA	DHAAPQIR-NH_2	8	905.48	7.755
DR3penA	DHα-(4-pentenyl)-ANPQIR-NH_2	8	1016.55	9.321
DR4penA	DHNα-(4-pentenyl)-APQIR-NH_2	8	1016.55	10.092

[a]Underlines indicate D-amino acid.
[b]Mass was calculated by ESI-MS.
[c]t_R (retention time) was measured by RP-HPLC.

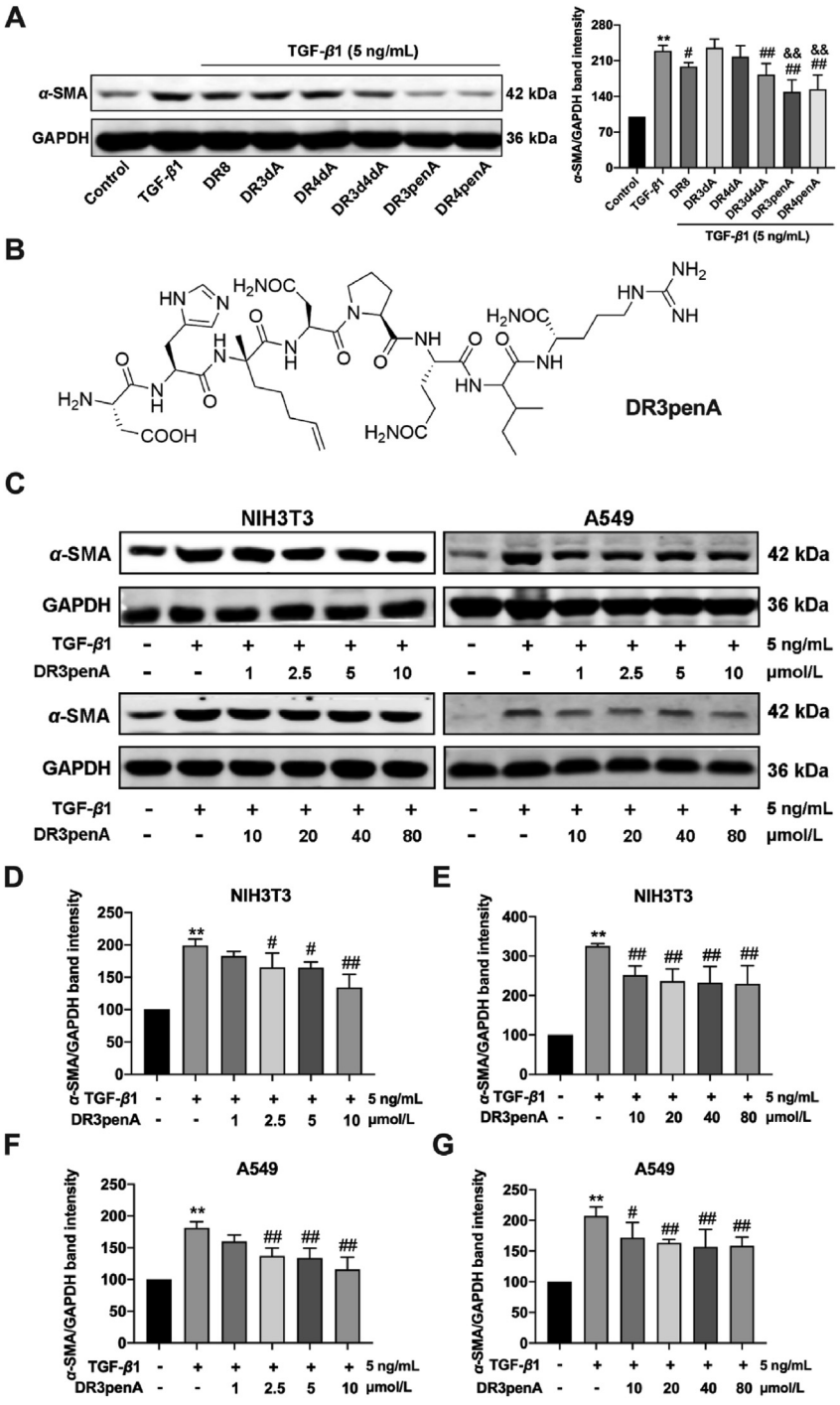

Figure 1 Activity screening of DR8 analogs and concentration optimizing of the peptide DR3penA. (A) α-SMA protein expression in TGF-β1-induced NIH3T3 cells after treatment with 80 μmol/L DR8 analogs. (B) Chemical structure of DR3penA. (C−G) α-SMA protein expression after DR3penA treatment at a concentration of 1−80 μmol/L in NIH3T3 and A549 cells. The data are presented as the mean ± SD ($n = 4$). $^{*}P < 0.05$, $^{**}P < 0.01$ *vs.* the control group; $^{\#}P < 0.05$, $^{\#\#}P < 0.01$ *vs.* the TGF-β1 group, $^{\&\&}P < 0.01$ *vs.* the DR8 group.

survival of mice induced by bleomycin (data not shown). Based on these results, DR3penA was selected to evaluate the antifibrotic activity.

To determine the effective concentration of DR3penA *in vitro*, different concentrations of DR3penA (1−80 μmol/L) were used to treat TGF-β1-induced NIH3T3 cells and A549 cells, and the expression level of α-SMA was assessed. The results demonstrated that α-SMA expression was obviously suppressed when the concentration of DR3penA reached 2.5 μmol/L in both cell lines (Fig. 1C−G). A previous activity study showed that the minimum effective concentrations of DR8 were 20 and 10 μmol/L in TGF-β1-induced NIH3T3 cells and A549 cells, respectively (Supporting Information Fig. S2). Additionally, DR3penA displayed no toxicity toward A549 cells when the concentration reached 160 μmol/L (Fig. S1B). Collectively, the results demonstrated that DR3penA displayed higher stability and better

Table 2 Half time ($t_{1/2}$) of DR8 and DR8 analogs in mice serum.

Peptide	$t_{1/2}$ (min)
DR8	70.19 ± 6.83
DR3penA	174.63 ± 31.66
DR4penA	270.65 ± 16.43

antifibrotic activity than DR8 *in vitro*. According to the concentration screening results, 2.5 and 10 μmol/L DR3penA were used in the follow-up *in vitro* experiments.

3.2. *DR3penA alleviates bleomycin-induced PF and collagen deposition in vitro and in vivo*

Since DR3penA displayed an inhibitory effect on the expression levels of α-SMA and collagen I *in vitro* (Supporting Information Fig. S3), we next assessed the antifibrotic activity of DR3penA *in vivo*. To confirm the influence of DR3penA on the lungs, mice were subcutaneously injected with DR3penA (2.5 mg/kg per day) for 21 days successively. HE staining and immunohistochemical analyses of SP-C protein showed that there were no pathological changes or damage to the alveolar structure of the lungs after DR3penA treatment (Supporting Information Fig. S4). Subsequently, bleomycin was injected intratracheally to establish an *in vivo* model of PF, and DR3penA was subcutaneously injected into mice at doses of 0.5 and 2.5 mg/kg. Pirfenidone, a clinically approved drug for PF treatment, was selected as a positive control to assess the antifibrotic activity of DR3penA in bleomycin-treated mice, because it has a good inhibitory effect in PF therapy. The gross anatomy of the lungs revealed that bleomycin-induced pathological changes, such as consolidation, edema, and hemorrhagic transformation, were obviously alleviated by administration of DR3penA (Fig. 2A). Moreover, DR3penA (0.5 or 2.5 mg/kg) also remarkedly decreased the lung coefficient and improved the survival and weight of mice (Fig. 2B−D). HE staining showed that DR3penA reduced bleomycin-induced pathological damage, including the destruction of lung structure, collapse of alveoli and infiltration of inflammatory cells (Fig. 2F).

Excessive ECM deposition in the lung interstitium leads to disorder of the lung matrix, which promotes the destruction of lung function and the formation of PF. ECM components, including collagen and fibronectin, were detected in lung tissues and cells. Masson staining and immunohistochemical analyses showed that DR3penA at a dose of 0.5 or 2.5 mg/kg significantly decreased collagen deposition and fibronectin expression in lungs of bleomycin-treated mice, and the inhibition of fibronectin was dose dependent (Fig. 2F−I). Consistently, *Col1a1* gene expression in the lungs was also downregulated by DR3penA (Fig. 2E). Together, the results showed that DR3penA effectively reduced the collagen deposition and attenuated PF progression in bleomycin-treated mice.

3.3. *DR3penA downregulates the expression of fibrotic markers in vitro and in vivo*

Given the effective inhibitory effect of DR3penA on bleomycin-induced collagen deposition and pathological damage in mice, the effect of DR3penA on the levels of fibrosis-associated proteins and genes was further evaluated *in vitro* and *in vivo*. Fibroblasts (NIH3T3) and lung epithelial cells (A549) were used to confirm the antifibrotic activity of DR3penA. α-SMA and fibronectin protein and gene expression and collagen I mRNA expression were notably downregulated by DR3penA at concentrations of 2.5 and 10 μmol/L in TGF-β1-induced NIH3T3 cells, and the decreases of gene expression (α-SMA, collagen I and fibronectin) and fibronectin protein expression were concentration dependent (Fig. 3A−C). As found in TGF-β1-induced A549 cells, the expression levels of proteins and genes involved in fibrosis (α-SMA, MMP-2, fibronectin and collagen I) were also suppressed after DR3penA (2.5 and 10 μmol/L) treatment. α-SMA protein and fibronectin mRNA levels were inhibited in a concentration-dependent manner (Fig. 3D−F). Consistent with the results in cells, α-SMA, MMP-2 and fibronectin expression were downregulated by DR3penA at a dose of 0.5 or 2.5 mg/kg in bleomycin-induced mice, and MMP2 protein expression was decreased in a dose-dependent manner (Fig. 3G−I). Taken together, our study confirmed that the peptide DR3penA can alleviate TGF-β1- and bleomycin-induced PF *in vitro* and *in vivo*.

3.4. *DR3penA inhibits ROS production in vitro and in vivo*

Given that DR8 exhibited antioxidant activity *in vitro* and *in vivo* and that the introduction of hydrophobic amino acids contributed to improved antioxidant activity[34], we speculated that DR3penA has an antioxidant effect against fibrotic progression. As shown in Fig. 4A, DR3penA reduced the level of intracellular ROS in TGF-β1-induced NIH3T3 cells and A549 cells. In addition, the levels of indicators related to oxidative stress in serum and lung tissues were measured. The results showed that the gene levels of *Nox1* and *Nox4*, which can produce ROS, were downregulated and those of antioxidant enzymes (*Sod1*, *Sod2* and *Cat*) were upregulated after DR3penA administration in bleomycin-induced PF mice (Fig. 4B). Consistently, DR3penA treatment reduced the level of MDA, which reflects the degree of oxidative stress, and elevated the activity of SOD and CAT in the serum of bleomycin-induced mice (Fig. 4C−E). The levels of *Cat* mRNA in lung tissues and MDA in serum were dose dependent. Collectively, all the above results demonstrated that DR3penA has an antioxidant effect on TGF-β1-induced oxidative injury of cells and bleomycin-induced oxidative stress in mice.

3.5. *Inhibitory effect of DR3penA on EMT and cell migration*

The role of EMT is mainly to promote the production of ECM secreted by mesenchymal cells and further drive organ fibrosis. Therefore, we next investigated whether DR3penA could alleviate PF by suppressing EMT *in vitro* and *in vivo*. The results showed that DR3penA at concentrations of 2.5 and 10 μmol/L significantly increased epithelial marker E-cadherin expression and inhibited mesenchymal marker Vimentin expression in A549 cells after TGF-β1 stimulation (Fig. 5A−C). Similarly, the immunofluorescence assay showed a consistent trend (Fig. 5G). In the *in vivo* study, DR3penA (0.5 or 2.5 mg/kg) upregulated E-cadherin protein and gene expression levels and downregulated vimentin expression in lung tissues, suggesting that DR3penA effectively repressed EMT in bleomycin-induced PF (Fig. 5D−F). Furthermore, cell migration assay was performed to verify the effect of DR3penA. As shown in Fig. 5H−K, the migration rate and the numbers of migrating cells were decreased prominently with DR3penA at doses of 0.5 and 2.5 mg/kg. Given all the above findings, we considered that the amelioration of PF by DR3penA may result from inhibition of EMT and the migration of epithelial cells.

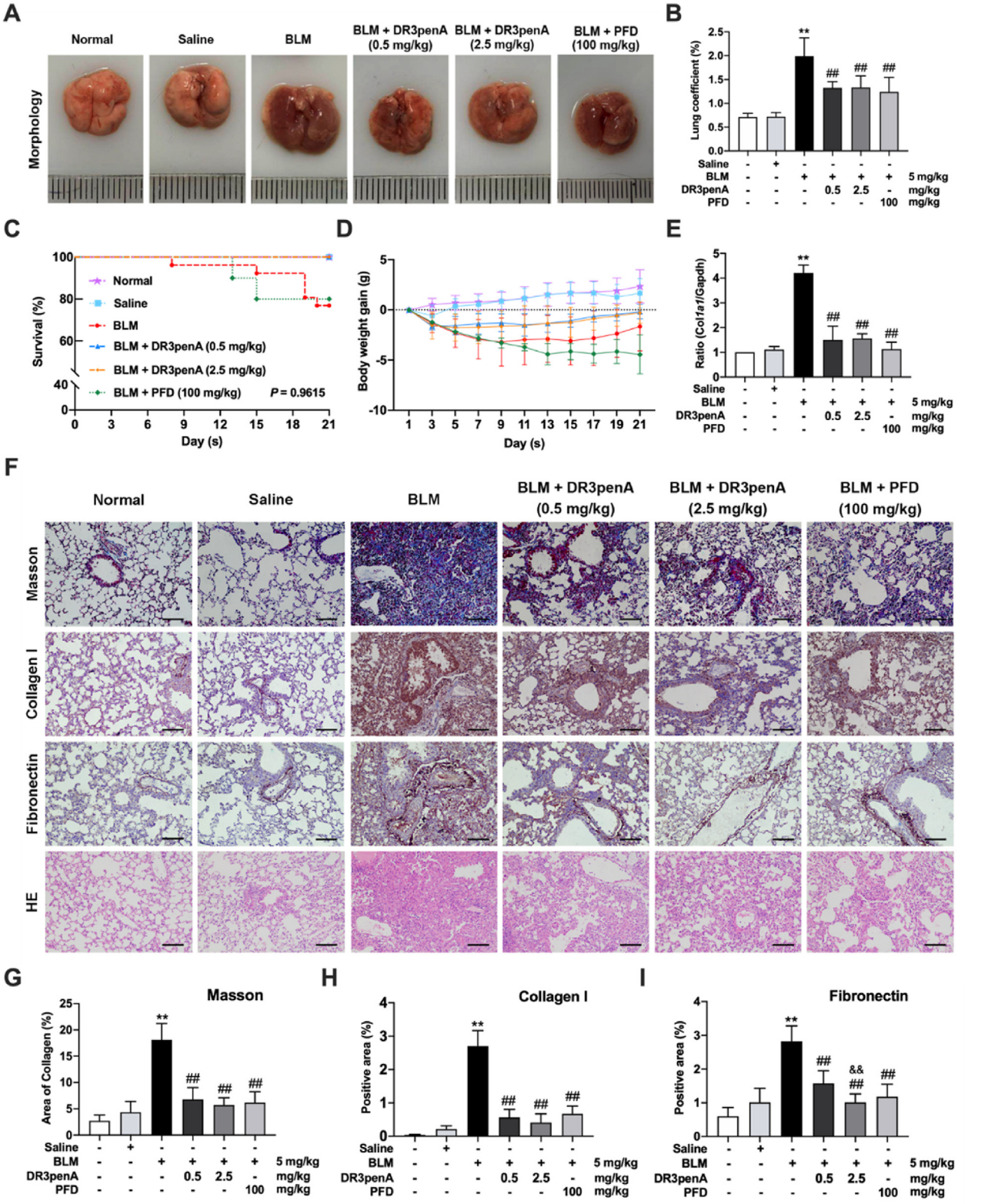

Figure 2 DR3penA alleviates bleomycin-induced PF and collagen deposition *in vitro* and *in vivo*. (A) Gross analyses of lungs in a mouse model after treatment with bleomycin, bleomycin plus DR3penA or PFD. (B) Lung coefficient of mice in the indicated groups. Survival rates (C) and body weights (D) of mice were measured and recorded during the experiment. (E) Real-time qPCR analysis of *Col1a1* mRNA expression in lung tissues. (F) Lung histopathology and collagen fibers were assessed by HE and Masson staining, respectively, and the protein levels of collagen I and fibronectin were examined by immunohistochemical staining (scale bars, 100 μm). (G) Quantitative analysis of the area of collagen fibers by Masson staining. Statistical analyses of the expression of collagen I (H) and fibronectin (I) measured by immunohistochemistry. The data are presented as the mean ± SD ($n = 8$). $^{*}P < 0.05$, $^{**}P < 0.01$ *vs*. the normal group; $^{\#}P < 0.05$, $^{\#\#}P < 0.01$ *vs*. the BLM group, $^{\&\&}P < 0.01$ *vs*. the DR3penA (0.5 mg/kg) group.

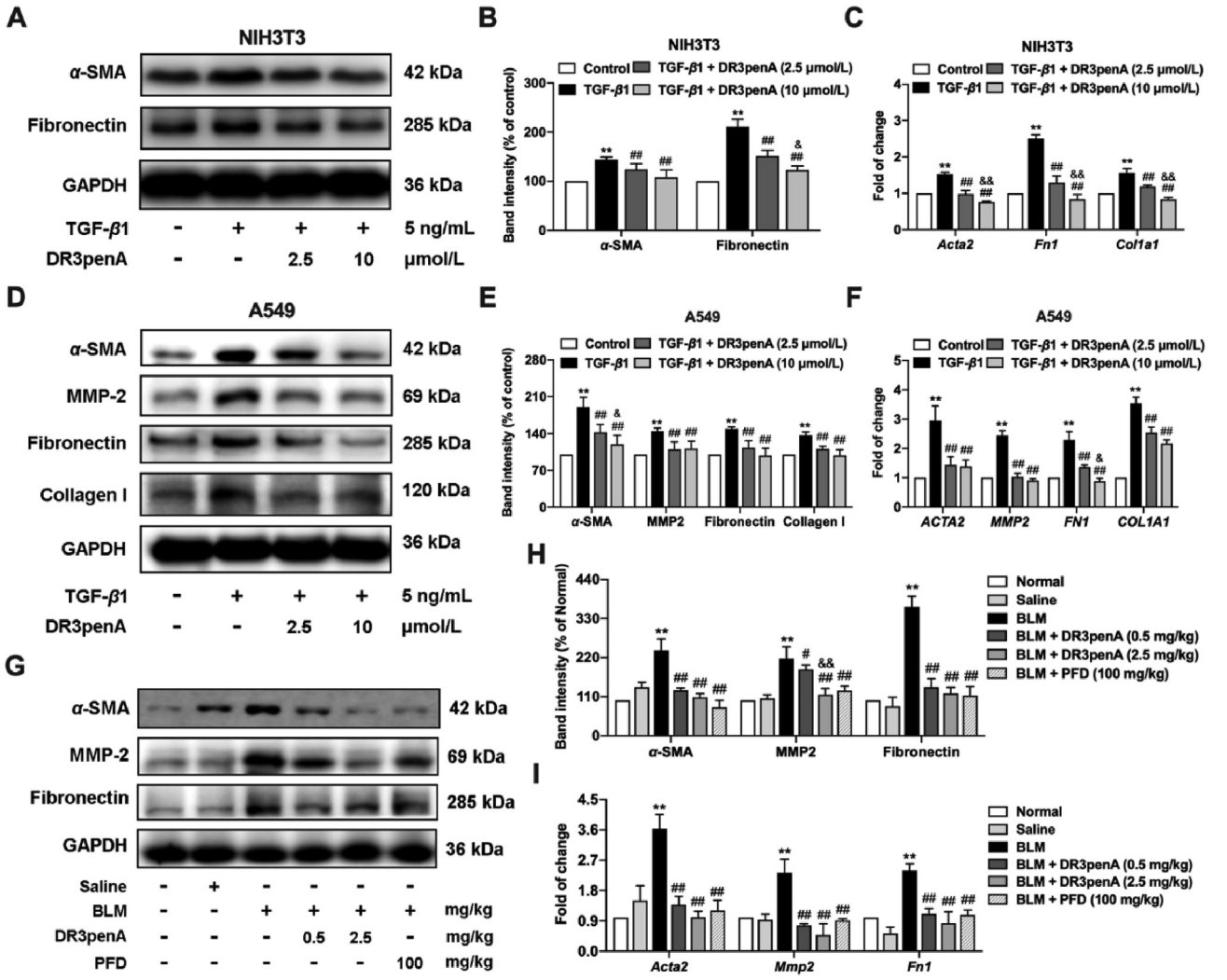

Figure 3 DR3penA downregulates the expression of fibrotic markers *in vitro* and *in vivo*. (A−B) α-SMA and fibronectin protein expression in TGF-β1-induced NIH3T3 cells after DR3penA treatment was detected and quantified *via* Western blotting. (C) The gene expression levels of *Acta2*, *Fn1* and *Col1a1* in NIIH3T3 cells were analyzed *via* real-time qPCR. (D−E) The protein levels of α-SMA, MMP-2, fibronectin and collagen I in TGF-β1-induced A549 cells after DR3penA treatment were assessed *via* Western blotting. (F) The gene levels of *ACTA2*, *MMP2*, *FN1* and *COL1A1* in A549 cells were determined by real-time qPCR analysis. (G−H) The protein expression levels of α-SMA, MMP-2 and fibronectin in bleomycin-induced mice after DR3penA or PFD administration were verified by Western blotting. (I) The mRNA transcription levels of *Acta2*, *Mmp2* and *Fn1* in mice in the indicated groups were determined by real-time qPCR assay. The data are presented as the mean ± SD ($n = 3$). $^{*}P < 0.05$, $^{**}P < 0.01$ *vs.* the normal group or control group; $^{\#}P < 0.05$, $^{\#\#}P < 0.01$ *vs.* the BLM group or the TGF-β1 group; $^{\&}P < 0.05$, $^{\&\&}P < 0.01$ *vs.* the DR3penA (0.5 mg/kg) group or the DR3penA (2.5 μmol/L) group.

3.6. DR3penA alleviates PF by downregulating miR-23b-5p expression

To explore the mechanism by which DR3penA alleviates PF, transcriptome sequencing technology was used to screen differentially expressed genes in the lung tissues of mice. The sequencing data analysis showed that 260 miRNAs were differentially expressed between the normal group and BLM group, of which 156 miRNAs were upregulated and 104 miRNAs were downregulated. Additionally, 121 miRNAs were differentially expressed between the DR3penA group and the model group, of which 65 miRNAs were upregulated and 56 miRNAs were downregulated (Fig. 6A−B). A Venn diagram showed that there were 56 miRNAs at the intersection of the two expression datasets (Fig. 6C). GO analysis of known miRNAs showed that the differentially expressed miRNAs were mainly involved in biological processes, such as biological regulation, metabolic process, developmental process, response to stimulus and localization (Supporting Information Fig. S5C). Cell composition showed that most of these miRNAs were located in organelles, membranes and extracellular regions (Fig. S5A). Moreover, molecular function analysis showed that these miRNAs are involved in binding, catalytic activity and signal transducer activity (Fig. S5B).

Based on the above results, miR-146-5p, miR-199-5p, miR-200a-3p, miR-23b-5p and miR-34a-5p were selected as candidate molecules, and the changes in the expression of these miRNAs were assessed in mice after treatment with bleomycin and DR3penA. The upregulation of miR-23b-5p and miR-34a-5p in mice induced by bleomycin was significantly inhibited after DR3penA (2.5 mg/kg) administration, and DR3penA presented a better inhibitory effect on

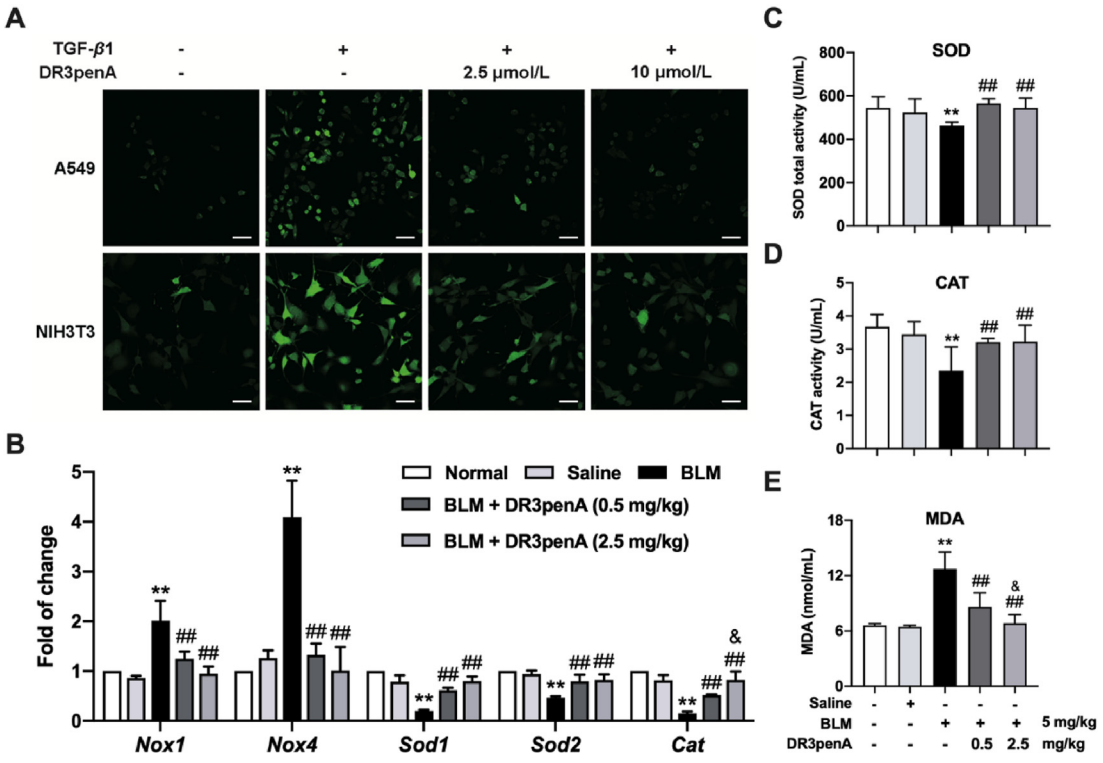

Figure 4 DR3penA inhibits oxidative injury *in vitro* and *in vivo*. (A) DCFH-DA staining for detection of the ROS level in TGF-β1-stimulated A549 cells and NIH3T3 cells after DR3penA treatment (scale bars, 50 μm). (B) *Nox1*, *Nox4*, *Sod1*, *Sod2* and *Cat* gene expression levels in bleomycin-treated mice after DR3penA administration. (C−E) SOD, CAT and MDA levels in the serum of mice after bleomycin, DR3penA and PFD administration. The data are presented as the mean ± SD ($n = 3$). $^{*}P < 0.05$, $^{**}P < 0.01$ *vs*. the normal group or control group; $^{\#}P < 0.05$, $^{\#\#}P < 0.01$ *vs*. the BLM group or the TGF-β1 group; $^{\&}P < 0.05$ *vs*. the DR3penA (0.5 mg/kg) group.

miR-23b-5p than miR-34a-5p (Fig. 6D). Consistently, DR3penA (10 μmol/L) significantly reduced miR-23b-5p expression in TGF-β1-induced A549 cells and NIH3T3 cells (Fig. 6E−F). Therefore, we considered that miR-23b-5p plays an important role in the progression of PF. To further confirm the inhibitory effect of DR3penA on PF *via* miR-23b-5p, the expression of fibrosis related proteins was evaluated after TGF-β1 induction and DR3penA treatment in A549 cells overexpressing miR-23b-5p. Compared with the NC group, the expression of miR-23b-5p was remarkedly increased, indicating that the transfection was effective (Fig. S5D). Furthermore, miR-23b-5p overexpression or TGF-β1 induction significantly elevated α-SMA, collagen I and fibronectin protein expression, and the increase induced by TGF-β1 was reduced by DR3penA. However, we observed that the effect of DR3penA was recovered in TGF-β1-induced cells after miR-23b-5p transfection (Fig. 6G). Together, these results indicate that DR3penA may alleviate PF by inhibiting the expression of miR-23b-5p.

3.7. DR3penA alleviates PF by regulating the MAPK/miR-23b-5p/AQP5 axis

Subsequently, the TargetScan and miRDB databases were used to predict the target genes of miR-23b-5p. The intersection of the databases is shown in Supporting Information Fig. S6A, from which eight possible targets of miR-23b-5p, namely, ABCA1, AQP5, CMTM4, GPX3, MTMR4, NKD1, SIRT5 and STK38, were selected for further assessment. The results showed that the expression of AQP5 was downregulated in A549 cells induced by TGF-β1, and the decrease was reversed by DR3penA at a concentration of 10 μmol/L (Supporting Information Fig. S6B). Comparable results were observed in bleomycin-induced mice, DR3penA (2.5 mg/kg) effectively decreased TGF-β1 expression and increased AQP5 expression (Fig. 7A). Furthermore, DR3penA recovered the gene expression of AQP5 in TGF-β1-induced A549 cells after miR-23b transfection (Fig. 7B). Base on the above results, we speculated that miR-23b-5p could regulate the expression level of AQP5. However, a dual luciferase reporter assay showed that the luciferase activity of AQP5-WT or AQP5-Mut was not obviously changed between the miR-23b-5p group and NC group (Fig. S6C−D), suggesting that AQP5 was not regulated by miR-23b-5p directly.

Previous studies reported that SB203580, SP600125 or shRNA-mediated gene silencing of p38 and JNK significantly increased the expression of AQP5, showing that the p38 and JNK signaling pathways inhibit the expression of AQP5[35]. To investigate the role of AQP5 in PF inhibited by DR3penA, the relationship between AQP5 and MAPK was further identified. Western blot analysis showed that AQP5 expression was elevated in TGF-β1-induced A549 cells pretreated with an ERK inhibitor (PD98059), indicating that the ERK pathway can suppress the expression of AQP5 (Fig. 7C). We further studied the signaling pathway that DR3penA might affect. DR3penA inhibited p38 and ERK phosphorylation *in vitro* and *in vivo*, suggesting that DR3penA might attenuate PF by suppressing the activation of TGF-β1/MAPK (Fig. 7D−E). Additionally, DR3penA inhibited the activation of the AKT and Smad pathways *in vitro* and *in vivo* (Supporting Information Fig. S7). Meanwhile, we found that miR-23b-5p expression was reduced in TGF-β1-induced cells after

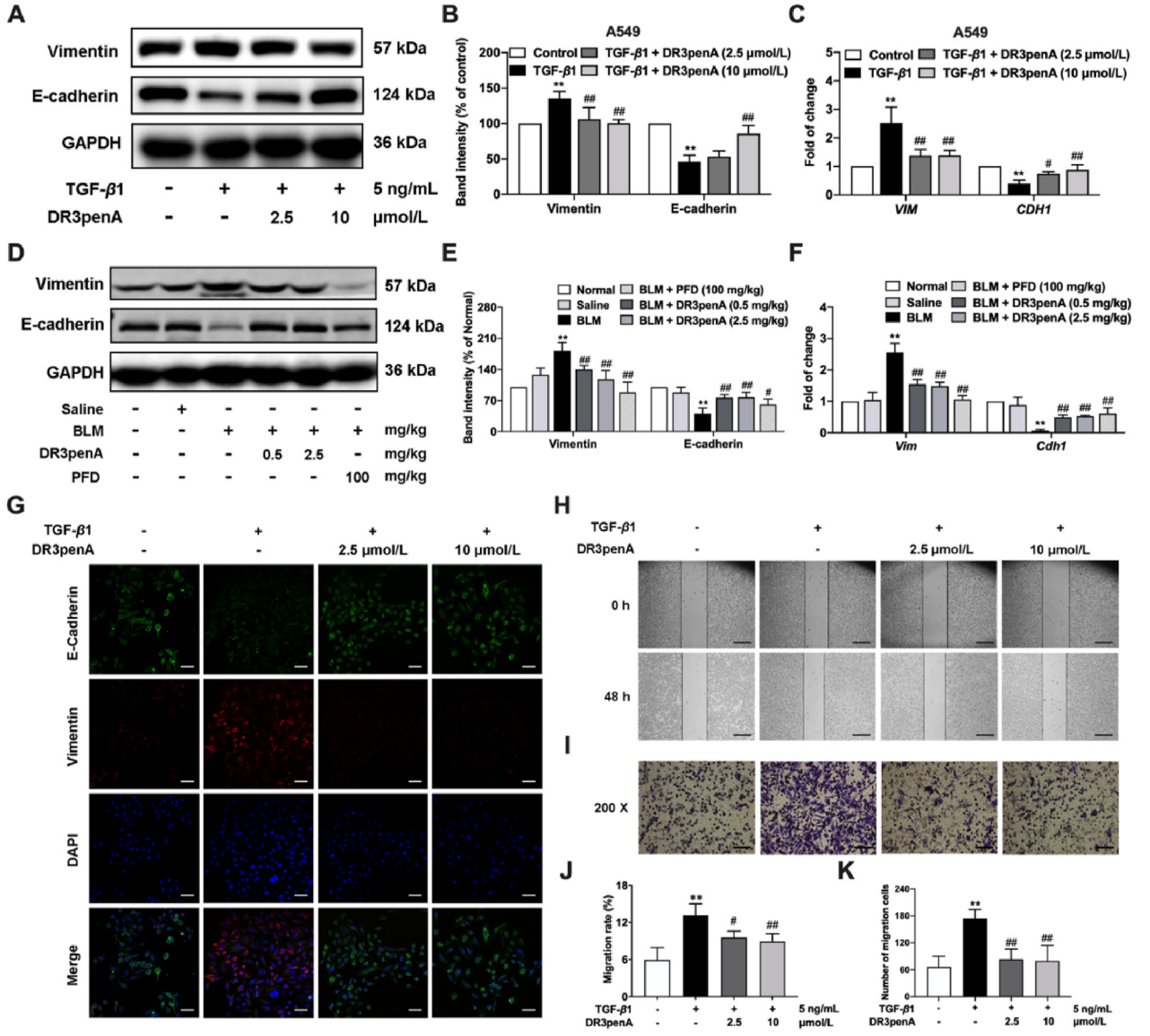

Figure 5 Inhibitory effect of DR3penA on EMT and cell migration. (A−B) Vimentin and E-cadherin protein levels in TGF-β1-stimulated A549 cells after DR3penA treatment were quantified *via* Western blotting. (C) *VIM* and *CDH1* gene levels in A549 cells were measured *via* real-time qPCR. (D−E) Vimentin and E-cadherin protein expression in bleomycin-induced mice after DR3penA or PFD administration was evaluated *via* Western blotting. (F) The mRNA transcription levels of *Vim* and *Cdh1* in mice in the indicated groups were determined by real-time qPCR. (G) Representative immunofluorescence images of A549 cells stained for vimentin (red) and E-cadherin (green) and with DAPI (blue) after TGF-β1 and/or DR3penA treatment (scale bars, 50 μm). (H) A scratch assay was performed in TGF-β1-induced A549 cells after DR3penA treatment (scale bars, 500 μm). (I) A Transwell chamber migration assay was used to evaluate the migration ability of A549 cells migration (scale bars, 100 μm). Statistical analysis of the migration rate (J) and number of migrating cells (K). The data are presented as the mean ± SD ($n = 3$). $^{*}P < 0.05$, $^{**}P < 0.01$ *vs*. the normal group or control group; $^{\#}P < 0.05$, $^{\#\#}P < 0.01$ *vs*. the BLM group or the TGF-β1 group.

treatment with PD98059 (ERK inhibitor) and SB203580 (p38 inhibitor), indicating that activation of the ERK and p38 pathways promoted miR-23b-5p expression (Supporting Information Fig. S8). Overall, DR3penA alleviates the progression of PF in part by directly regulating MAPK/miR-23b-5p/AQP5.

3.8. *Acute toxicity evaluation of DR3penA*

To clarify the safety range of the therapeutic dosage and possible adverse reactions, an acute toxicity test was performed to evaluate the safety of DR3penA after single dosage treatments. The results showed that DR3penA at a dose of 0.5−62.5 mg/kg exhibited no obvious toxicity with regard to mortality, weight, organ coefficient or liver and kidney function, while DR8 had a negative effect on liver and renal function (Supporting Information Figs. S9−S10 and Tables S1−S2). Since no mice died when the dosage of DR3penA reached 62.5 mg/kg, a dosage of 5000 mg/kg was used to verify the toxicity of DR3penA according to the globally harmonized classification system (GHS) (Supporting Information Table S5). The results showed that there were no abnormal

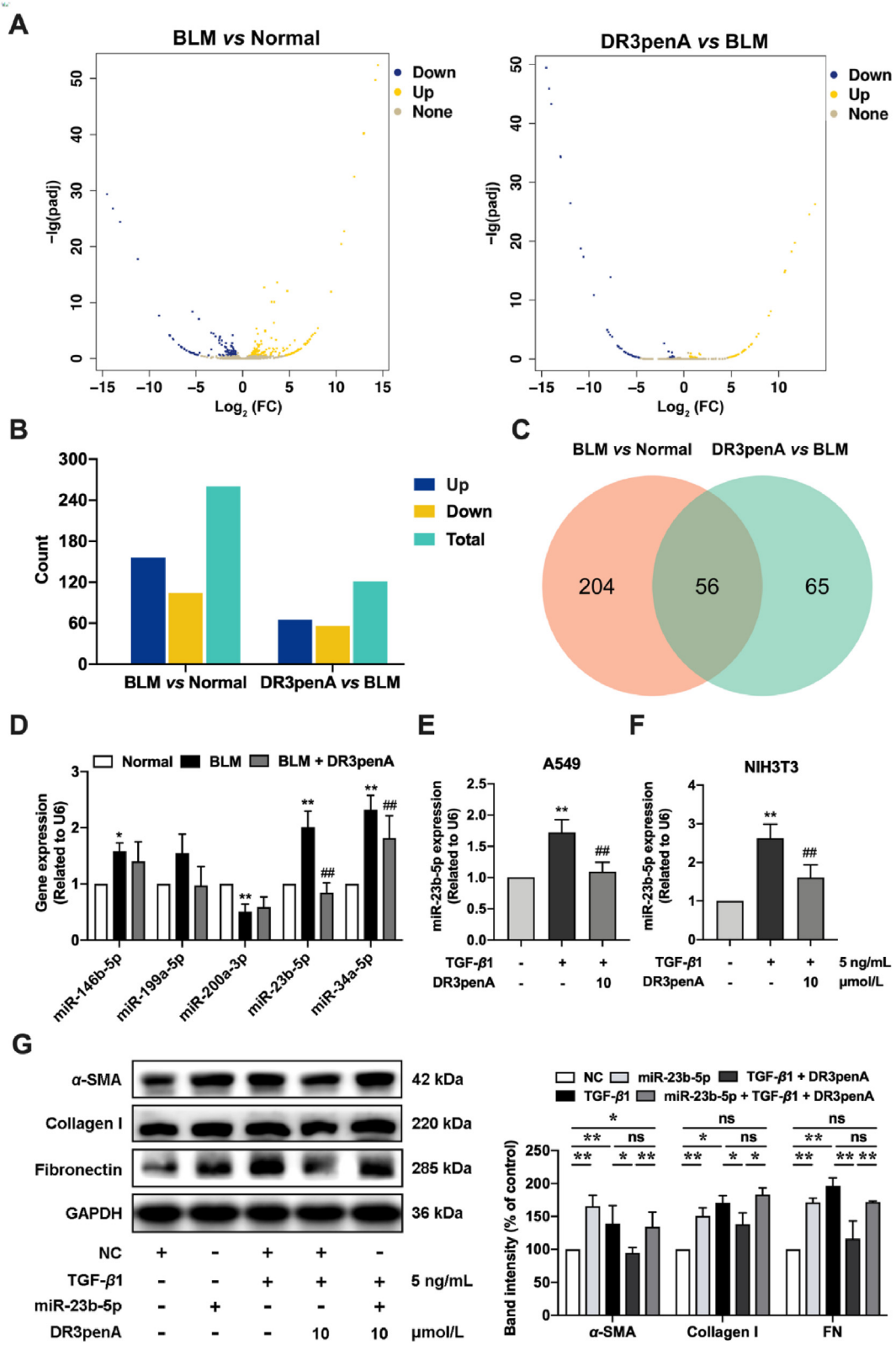

Figure 6 DR3penA alleviates PF by downregulating miR-23b-5p expression. (A) Volcano plots of miRNA expression showing upregulated (yellow) and downregulated genes (blue). (B) The numbers of upregulated and downregulated miRNAs. (C) Venn diagram showing the numbers of differentially expressed miRNAs between the BLM group and normal group and between the DR3penA group and BLM group as well as the overlapping miRNAs. (D) The effect of DR3penA on different miRNA expression levels in bleomycin-induced PF mice. The effect of DR3penA on miR-23b-5p expression in TGF-β1-induced A549 cells (E) and NIH3T3 cells (F). (G) The protein expression levels of α-SMA, collagen I and fibronectin in TGF-β1-induced A549 cells treated with DR3penA were detected *via* Western blotting. The data are presented as the mean ± SD ($n = 3$). $^{*}P < 0.05$, $^{**}P < 0.01$ *vs.* the normal group or control group; $^{\#}P < 0.05$, $^{\#\#}P < 0.01$ *vs.* the BLM group or the TGF-β1 group.

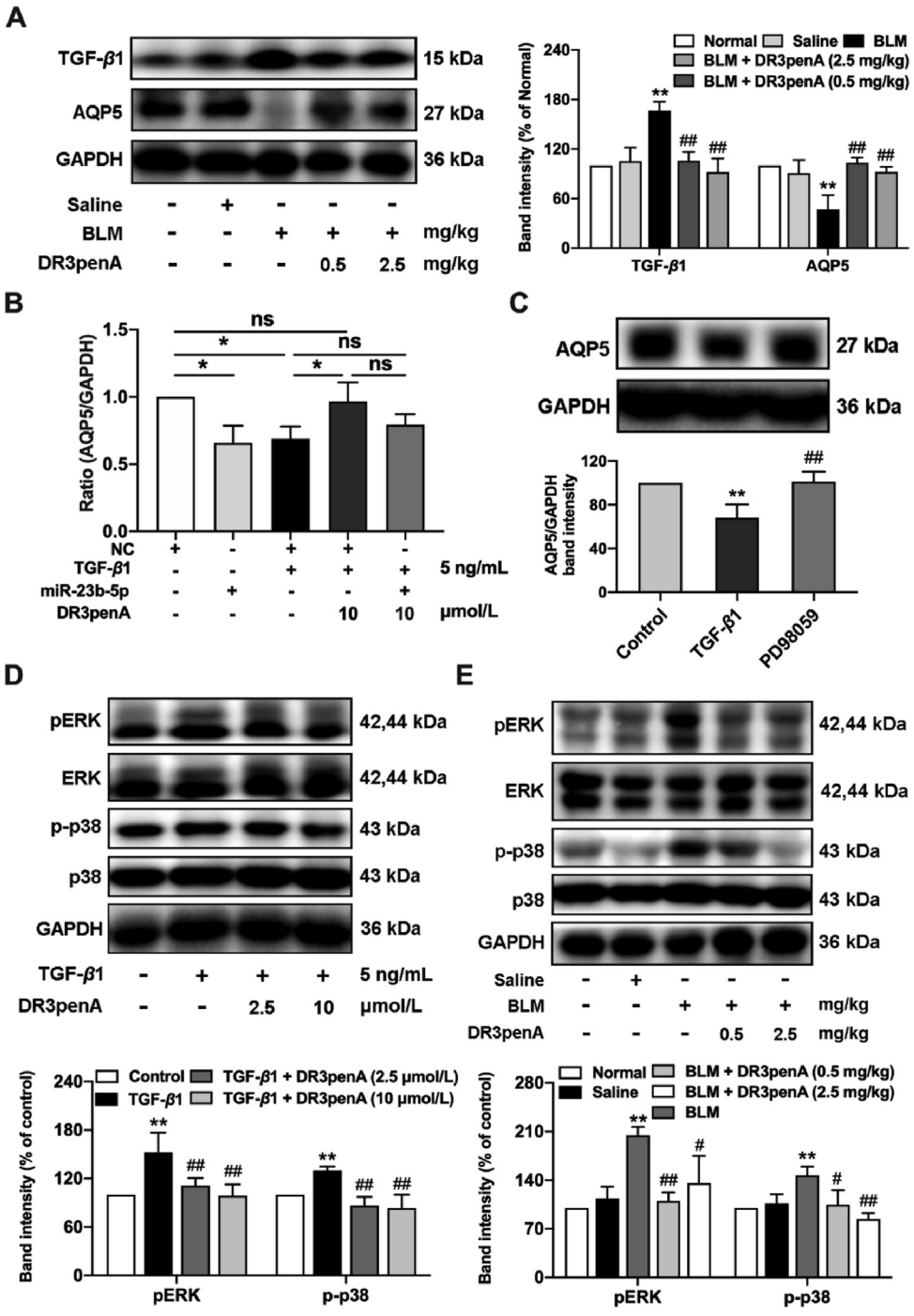

Figure 7 DR3penA alleviates PF by regulating the MAPK/miR-23b-5p/AQP5 axis. (A) TGF-β1 and AQP5 protein levels in bleomycin-induced PF mice treated with DR3penA were determined by Western blot analysis. (B) The effect of DR3penA on the level of *AQP5* mRNA in A549 cells over-expressing miR-23b-5p or induced with TGF-β1. (C) The expression of AQP5 in TGF-β1-induced A549 cells pretreated with 10 μmol/L PD98059 (ERK inhibitor) was analyzed *via* Western blotting. ERK and p38 phosphorylation in TGF-β1-induced A549 cells (D) and bleomycin-induced mice (E) was measured *via* Western blotting. pERK1/2 and p-p38 were normalized to total ERK and p38, respectively. The data are presented as the mean ± SD ($n = 3$). $^{*}P < 0.05$, $^{**}P < 0.01$ *vs*. the normal group or control group; $^{\#}P < 0.05$, $^{\#\#}P < 0.01$ *vs*. the BLM group or the TGF-β1 group.

symptoms or deaths among female or male mice after DR3penA treatment (Table 3). Gross anatomy revealed no obvious abnormality in the appearances of hearts, livers, lungs and kidneys in female and male mice as well as the spleens in female mice after DR3penA administration, whereas the spleens in male mice were swollen (Fig. 8A). Similarly, the organ coefficients (heart, liver, lung and kidney) were not significantly different after DR3penA treatment, while the spleen coefficient was markedly elevated in male mice compared with the PBS control group (Fig. 8G−K). Pathological examination showed that there were no abnormal lesions in kidney and lung tissues after DR3penA administration, while there were a few inflammatory cell infiltration and slight

edema in liver tissues after DR3penA and PBS administration (Fig. 8B). We considered that the slight inflammatory reaction in livers may be caused by the growth environment and feeding conditions of the Kunming mice. Liver and renal function were assessed, and there was no remarkable difference between the PBS and DR3penA groups (Fig. 8C−F). As there were no deaths among the mice after DR3penA treatment at a dose of 5000 mg/kg, the toxicity of DR3penA was assigned as unclassified according to the GHS standard, indicating that DR3penA is a peptide drug without obvious toxicity or acute side effects and that its safety is greater than that of DR8.

4. Discussion

Our previous study revealed that the stability and antifibrotic activity were increased after residues Asn3 and Asn4 of DR8 were substituted by D-amino acids and alanine, respectively. It is likely that D-amino acids cannot be recognized by proteases in mammals and that alanine replacement changed the steric hindrance and improved the hydrophobicity of the peptide[33,34,36−40]. Studies have shown that the introduction of α-(4-pentenyl)-Ala into peptide Feleucin-K3 improved its antimicrobial activity and stability[41,42]. Based on the aforementioned findings, unnatural hydrophobic alanine (α-(4-pentenyl)-Ala and D-Ala) was selected to replace residues Asn3 and Asn4 of DR8. Activity screening and stability assays showed that the half-life of the analog DR3penA in serum was prolonged from 70.19 ± 6.83 to 174.63 ± 31.66 min and that the effective concentration of DR3penA was reduced from 80 to 2.5 μmol/L *in vitro*. We speculated that the quaternary carbon structure and long hydrophobic fatty chain of α-(4-pentenyl)-Ala improved the stability of the peptide and thar the enhanced hydrophobicity of DR3penA may increase the antioxidant activity of the peptide and promote the entry of the peptide into cells[34,43,44]. To prove this hypothesis, we compared the ROS-scavenging ability of DR8 and DR3penA in A549 cells and NIH3T3 cells using DCFH-DA fluorescent probe. The results confirmed that the antioxidant activity of DR3penA was obviously enhanced compared with DR8, indicating that increased antioxidative ability of DR3penA contributed to the improved antifibrotic activity (Supporting Information Fig. S11). EMT and oxidative stress are important in the pathogenesis of PF. ROS participate in regulation of the EMT process by regulating miRNA expression and activating multiple EMT-related transcription factors and signaling pathways[45]. In a further activity study, DR3penA displayed an inhibitory effect on oxidative stress, EMT and the ECM deposition pathway *in vitro* and *in vivo*, indicating that DR3penA has high activity in alleviating PF. Notably, the peptide DR3penA displayed led to improved survival of mice and had an equivalent effect on ameliorating pathological damage and ECM deposition compared with the positive control pirfenidone. Meanwhile, a lower dosage was required for DR3penA than for pirfenidone, indicating an advantage of the peptide DR3penA in effective dosage compared with pirfenidone.

miR-23b-5p is involved in regulating the development of various diseases. Research has shown that miR-23b-5p promotes tumor growth in the kidney by targeting proline oxidase, which increases the production of ROS and thus suppresses tumor cell apoptosis[46]. Moreover, miR-23b-5p induced apoptosis of glioma cells and increased chemoresistance to temozolomide in glioma by targeting Toll-like receptor 4 (TLR4)[47]. In this study, for the first time, miR-23b-5p was identified as a profibrogenic gene in PF. Transcriptome sequencing revealed that miR-23b-5p was highly expressed in bleomycin-treated mice and that the upregulation was decreased in the DR3penA administration group. Experimental validation confirmed that DR3penA decelerated the progression of PF by inhibiting miR-23b-5p expression, which provides a new approach for further mechanistic research and a potential therapeutic target for PF.

AQP5 mainly mediates the selective transmembrane transport of water in multiple organs and provides necessary systematic regulation to maintain the water balance throughout the whole body. In radiation-, hydrogen sulfide-, lipopolysaccharide-, and *Pseudomonas aeruginosa*-induced ALI, decreased expression of AQP5 destroyed the barrier function of epithelial cells and aggravated lung injury[48−51]. Several studies have suggested that AQP5 expression is decreased in a bleomycin-induced PF model, which may be due to the persistent injury of alveolar epithelial cells caused by lung injury and inflammation[19,52,53]. Our results showed that DR3penA significantly inhibited the downregulation of AQP5 induced by bleomycin in mice and TGF-β1 in

Table 3 Body weight of mice after DR3penA (5000 mg/kg) administration (mean ± SD, $n = 5$).

Day	Mice	Weight (g)	
		PBS	DR3penA (5000 mg/kg)
0	Female	15.60 ± 0.20	16.20 ± 0.69
	Male	15.15 ± 0.34	15.60 ± 0.45
1	Female	19.20 ± 0.61	19.99 ± 1.37
	Male	19.72 ± 0.22	19.47 ± 0.96
3	Female	23.70 ± 0.94	24.21 ± 1.59
	Male	25.13 ± 0.46	23.63 ± 1.23
5	Female	25.24 ± 1.13	27.51 ± 2.24
	Male	26.86 ± 0.30	27.86 ± 1.45
7	Female	27.67 ± 1.52	31.44 ± 2.09*
	Male	30.05 ± 0.55	32.82 ± 1.87**
9	Female	27.63 ± 2.10	32.26 ± 1.60**
	Male	32.64 ± 0.58	31.72 ± 1.23
11	Female	29.40 ± 2.22	34.49 ± 2.39**
	Male	35.32 ± 0.57	37.12 ± 1.60
13	Female	31.00 ± 2.39	35.58 ± 1.69**
	Male	37.00 ± 0.59	38.90 ± 1.81*

*$P < 0.05$, **$P < 0.01$ *vs.* the PBS control group.

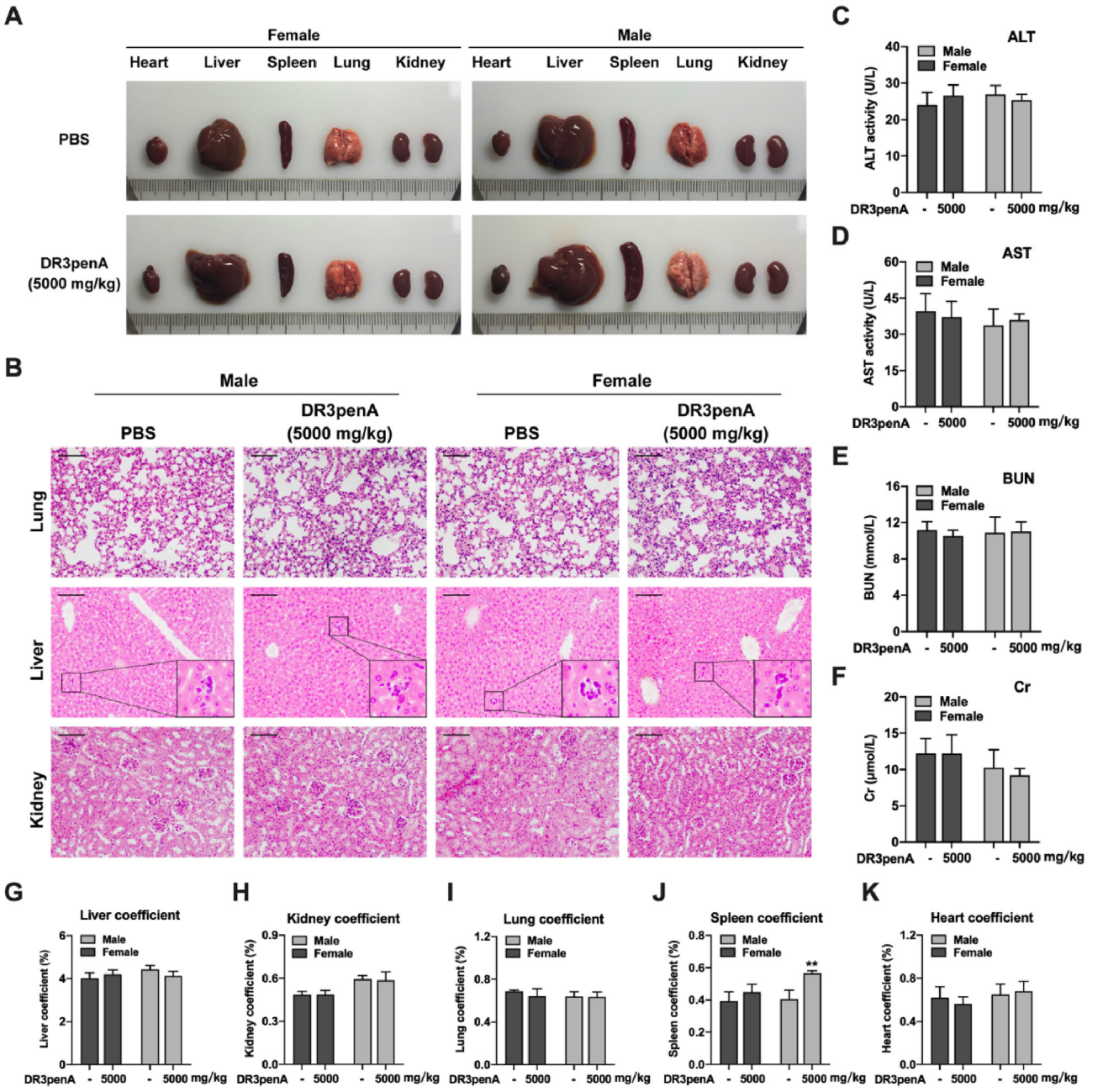

Figure 8 Acute toxicity evaluation of DR3penA. (A) Gross analyses of hearts, livers, spleens, lungs and kidneys after DR3penA administration. (B) HE staining of livers, kidneys and lungs after DR3penA administration (scale bars, 100 μm). ALT activity (C), AST activity (D), BUN level (E) and Cr level (F) in mice after DR3penA administration. Liver (G), kidney (H), lung (I), spleen (J) and heart (K) coefficients in mice after DR3penA administration. The data are presented as the mean ± SD ($n = 5$). *$P < 0.05$, **$P < 0.01$ *vs*. the PBS group.

A549 cells, indicating that DR3penA reduced the damage to epithelial cells by restoring the expression of AQP5. Although AQP5 was not found to be a direct target of miR-23b-5p, AQP5 was demonstrated to be negatively regulated by miR-23b-5p. The MAPK pathway is activated in PF models induced by bleomycin, silica, paraquat, cigarette smoke and radiation[54–58]. It was reported that the activation of p38 and JNK downregulated the expression AQP5[35], and we found that DR3penA inhibited activation of the ERK and p38 pathways, indicating that DR3penA may decrease the expression of AQP5 by blocking the MAPK pathway. Additionally, TGF-β1 upregulated the expression of miR-23b-5p by inhibiting the ERK and p38 pathways. Taken together, DR3penA may alleviate PF by regulating the MAPK/miR-23b-5p/AQP5 pathway.

The safety of drugs is a key factor in determining whether new drugs can enter clinical trials from preclinical research; meanwhile, it is of great significance for further optimization of the structure of compounds, improving druggability and obtaining safe and effective candidate drugs. In this study, although the spleens of male mice were swollen after DR3penA administration at a dose of 5000 mg/kg, DR3penA showed no obvious toxicity toward other organs (lung, liver, kidney and heart) or kidney and

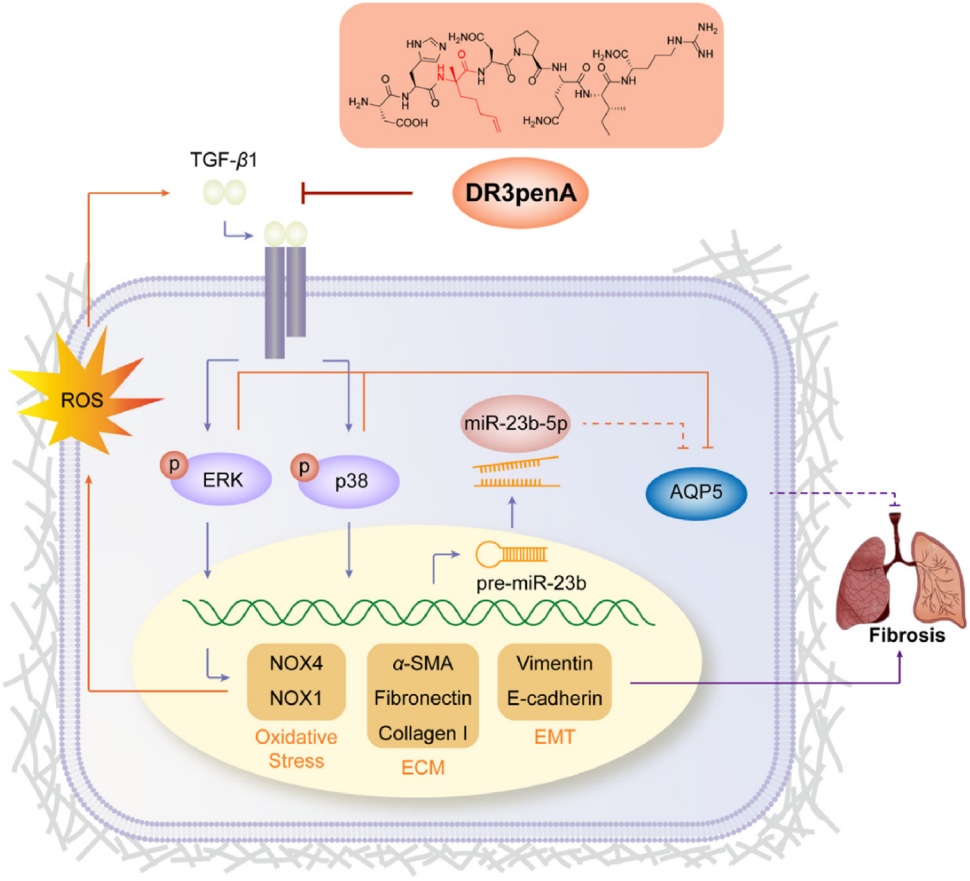

Figure 9 Schematic showing the mechanism by which the peptide DR3penA improves PF. DR3penA inhibits miR-23b-5p expression by suppressing the TGF-β1-induced ERK and p38 signaling pathways, which further upregulates the level of AQP and alleviates PF. Meanwhile, DR3penA suppresses TGF-β1-induced oxidative stress and EMT by inhibiting the ERK and p38 signaling pathways, resulting in improvement of PF.

liver functions in mice. However, DR8 showed toxic effects in the liver and kidney at a dose of 0.5 mg/kg, suggesting that the peptide DR3penA has a significantly improved safety profile. These results suggest that DR3penA is a peptide drug without obvious toxicity or acute side effects and has a distinct safety advantage compared with DR8.

5. Conclusions

In conclusion, this study showed that the novel peptide DR3penA modified by the unnatural amino acid α-(4-pentenyl)-Ala has potent anti-pulmonary fibrotic activity, high stability and low toxicity. Meanwhile, DR3penA has the advantages of a lower dosage and higher safety while possessing equivalent activity in alleviating PF compared with pirfenidone. Additionally, miR-23b-5p was identified as a profibrogenic gene in PF for the first time, which provides a potential therapeutic target for PF. Further mechanistic studies indicated that DR3penA effectively attenuates PF by regulating MAPK/miR-23b-5p/AQP5 (Fig. 9). Therefore, the peptide DR3penA can be further studied as a candidate compound for the treatment of PF.

Acknowledgments

This study was supported by the CAMS Innovation Fund for Medical Sciences (CIFMS, Nos. 2019-I2M-5-074, 2021-I2M-1-026, 2021-I2M-3-001, 2022-I2M-2-002, China), the Program for the Ministry of Education "Peptide Drugs" Innovation Team (No. IRT_15R27, China) and the Fundamental Research Funds for the Central Universities (No. lzujbky-2021-it17, China).

Author contributions

Junqiu Xie and Rui Wang designed and supervised the project and provided financial support. Dan Wang performed the experiments and drafted the original manuscript. Bochuan Deng and Lu Cheng analyzed the data and revised the manuscript. Jieru Li, Jiao Zhang and Xiang Zhang helped to perform the animal experiment. Xiaomin Guo and Tiantian Yan helped to perform the cellular experiments. Xin Yue and Yingying An conducted peptide synthesis. Bangzhi Zhang and Wenle Yang reviewed the manuscript.

Conflicts of interest

The authors declare that they have no financial or non-financial potential conflicts of interest.

Appendix A. Supporting information

Supporting data to this article can be found online at https://doi.org/10.1016/j.apsb.2022.09.001.

References

1. Richeldi L, du Bois RM, Raghu G, Azuma A, Brown KK, Costabel U, et al. Efficacy and safety of nintedanib in idiopathic pulmonary fibrosis. *N Engl J Med* 2014;**370**:2071−82.
2. Galli JA, Pandya A, Vega-Olivo M, Dass C, Zhao H, Criner GJ. Pirfenidone and nintedanib for pulmonary fibrosis in clinical practice: tolerability and adverse drug reactions. *Respirology* 2017;**22**:1171−8.
3. Wynn TA. Common and unique mechanisms regulate fibrosis in various fibroproliferative diseases. *J Clin Investig* 2007;**117**:524−9.
4. Scotton CJ, Chambers RC. Molecular targets in pulmonary fibrosis: the myofibroblast in focus. *Chest* 2007;**132**:1311−21.
5. Liu G, Beri R, Mueller A, Kamp DW. Molecular mechanisms of asbestos-induced lung epithelial cell apoptosis. *Chem Biol Interact* 2010;**188**:309−18.
6. Radisky DC, Levy DD, Littlepage LE, Liu H, Nelson CM, Fata JE, et al. Rac1b and reactive oxygen species mediate MMP-3-induced EMT and genomic instability. *Nature* 2005;**436**:123−7.
7. Cucoranu I, Clempus R, Dikalova A, Phelan PJ, Ariyan S, Dikalov S, et al. NAD(P)H oxidase 4 mediates transforming growth factor-beta1-induced differentiation of cardiac fibroblasts into myofibroblasts. *Circ Res* 2005;**97**:900−7.
8. Daniil ZD, Papageorgiou E, Koutsokera A, Kostikas K, Kiropoulos T, Papaioannou AI, et al. Serum levels of oxidative stress as a marker of disease severity in idiopathic pulmonary fibrosis. *Pulm Pharmacol Ther* 2008;**21**:26−31.
9. Bueno MJ, Perez de Castro I, Malumbres M. Control of cell proliferation pathways by microRNAs. *Cell Cycle* 2008;**7**:3143−8.
10. Inui M, Martello G, Piccolo S. MicroRNA control of signal transduction. *Nat Rev Mol Cell Biol* 2010;**11**:252−63.
11. Abba ML, Patil N, Leupold JH, Allgayer H. MicroRNA regulation of epithelial to mesenchymal transition. *J Clin Med* 2016;**5**:8.
12. Pandit KV, Corcoran D, Yousef H, Yarlagadda M, Tzouvelekis A, Gibson KF, et al. Inhibition and role of let-7d in idiopathic pulmonary fibrosis. *Am J Respir Crit Care Med* 2010;**182**:220−9.
13. Fierro-Fernandez M, Busnadiego O, Sandoval P, Espinosa-Diez C, Blanco-Ruiz E, Rodriguez M, et al. miR-9-5p suppresses pro-fibrogenic transformation of fibroblasts and prevents organ fibrosis by targeting NOX4 and TGFBR2. *EMBO Rep* 2015;**16**:1358−77.
14. Boureima Oumarou D, Ji H, Xu J, Li S, Ruan W, Xiao F, et al. Involvement of microRNA-23b-5p in the promotion of cardiac hypertrophy and dysfunction via the HMGB2 signaling pathway. *Biomed Pharmacother* 2019;**116**:108977.
15. Cheng H, Ding J, Tang G, Huang A, Gao L, Yang J, et al. Human mesenchymal stem cells derived exosomes inhibit the growth of acute myeloid leukemia cells *via* regulating miR-23b-5p/TRIM14 pathway. *Mol Med* 2021;**27**:128.
16. You L, Wang Y, Gao Y, Wang X, Cui X, Zhang Y, et al. The role of microRNA-23b-5p in regulating brown adipogenesis and thermogenic program. *Endocr Connect* 2020;**9**:457−70.
17. Hu GD, Wang CX, Wang HY, Wang YQ, Hu S, Cao ZW, et al. Long noncoding RNA CCAT2 functions as a competitive endogenous RNA to regulate FOXC1 expression by sponging miR-23b-5p in lung adenocarcinoma. *J Cell Biochem* 2018;**120**:7998−8007.
18. Vassiliou AG, Manitsopoulos N, Kardara M, Maniatis NA, Orfanos SE, Kotanidou A. Differential expression of aquaporins in experimental models of acute lung injury. *In Vivo* 2017;**31**:885−94.
19. Gao X, Wang G, Zhang W, Peng Q, Xue M, Jinhong H. Expression of pulmonary aquaporin 1 is dramatically upregulated in mice with pulmonary fibrosis induced by bleomycin. *Arch Med Sci* 2013;**9**:916−21.
20. Krane CM, Deng B, Mutyam V, McDonald CA, Pazdziorko S, Mason L, et al. Altered regulation of aquaporin gene expression in allergen and IL-13-induced mouse models of asthma. *Cytokine* 2009;**46**:111−8.
21. Wang K, Feng YL, Wen FQ, Chen XR, Ou XM, Xu D, et al. Decreased expression of human aquaporin-5 correlated with mucus overproduction in airways of chronic obstructive pulmonary disease. *Acta Pharmacol Sin* 2007;**28**:1166−74.
22. Song T, Yang H, Ho JC, Tang SC, Sze SC, Lao L, et al. Expression of aquaporin 5 in primary carcinoma and lymph node metastatic carcinoma of non-small cell lung cancer. *Oncol Lett* 2015;**9**:2799−804.
23. Lee SJ, Chae YS, Kim JG, Kim WW, Jung JH, Park HY, et al. AQP5 expression predicts survival in patients with early breast cancer. *Ann Surg Oncol* 2014;**21**:375−83.
24. Ma T, Fukuda N, Song Y, Matthay MA, Verkman AS. Lung fluid transport in aquaporin-5 knockout mice. *J Clin Investig* 2000;**105**:93−100.
25. Apostolopoulos V, Bojarska J, Chai TT, Elnagdy S, Kaczmarek K, Matsoukas J, et al. A global review on short peptides: frontiers and perspectives. *Molecules* 2021;**26**:430.
26. Conibear AC, Schmid A, Kamalov M, Becker CFW, Bello C. Recent advances in peptide-based approaches for cancer treatment. *Curr Med Chem* 2020;**27**:1174−205.
27. Lau JL, Dunn MK. Therapeutic peptides: historical perspectives, current development trends, and future directions. *Bioorg Med Chem* 2018;**26**:2700−7.
28. Angell Y, Holford M, Moos WH. Building on success: a bright future for peptide therapeutics. *Protein Pept Lett* 2018;**25**:1044−50.
29. Al-Khayri JM, Asghar W, Khan S, Akhtar A, Ayub H, Khalid N, et al. Therapeutic potential of marine bioactive peptides against human immunodeficiency virus: recent evidence, challenges, and future trends. *Mar Drugs* 2022;**20**:477.
30. Wang D, Yan Z, Bu L, An C, Deng B, Zhang J, et al. Protective effect of peptide DR8 on bleomycin-induced pulmonary fibrosis by regulating the TGF-beta/MAPK signaling pathway and oxidative stress. *Toxicol Appl Pharmacol* 2019;**382**:114703.
31. Xu HJ, Hong SH, Yan ZB, Zhao Q, Shi Y, Song NZ, et al. RAP-8 ameliorates liver fibrosis by modulating cell cycle and oxidative stress. *Life Sci* 2019;**229**:200−9.
32. Deng B, Yang W, Wang D, Cheng L, Bu L, Rao J, et al. Peptide DR8 suppresses epithelial-to-mesenchymal transition *via* the TGF-beta/MAPK signaling pathway in renal fibrosis. *Life Sci* 2020;**261**:118465.
33. Wang D, Cheng L, Li J, Deng B, Yan T, Yue X, et al. Peptide DR8 analogs alleviate pulmonary fibrosis *via* suppressing TGF-beta1 mediated epithelial-mesenchymal transition and ERK1/2 pathway *in vivo* and *in vitro*. *Eur J Pharm Sci* 2021;**167**:106009.
34. Zou TB, He TP, Li HB, Tang HW, Xia EQ. The structure−activity relationship of the antioxidant peptides from natural proteins. *Molecules* 2016;**21**:72.
35. Chen HH, Zhou XL, Shi YL, Yang J. Roles of p38 MAPK and JNK in TGF-beta1-induced human alveolar epithelial to mesenchymal transition. *Arch Med Res* 2013;**44**:93−8.
36. Khara JS, Priestman M, Uhia I, Hamilton MS, Krishnan N, Wang Y, et al. Unnatural amino acid analogues of membrane-active helical peptides with anti-mycobacterial activity and improved stability. *J Antimicrob Chemother* 2016;**71**:2181−91.
37. Knappe D, Henklein P, Hoffmann R, Hilpert K. Easy strategy to protect antimicrobial peptides from fast degradation in serum. *Antimicrob Agents Chemother* 2010;**54**:4003−5.
38. Meng H, Kumar K. Antimicrobial activity and protease stability of peptides containing fluorinated amino acids. *J Am Chem Soc* 2007;**129**:15615−22.
39. Kim JW, Kim TD, Hong BS, Kim OY, Yoon WH, Chae CB, et al. A serum-stable branched dimeric anti-VEGF peptide blocks tumor growth *via* anti-angiogenic activity. *Exp Mol Med* 2010;**42**:514−23.
40. Yoo SA, Bae DG, Ryoo JW, Kim HR, Park GS, Cho CS, et al. Arginine-rich anti-Vascular endothelial growth factor (anti-VEGF) hexapeptide inhibits collagen-induced arthritis and VEGF-stimulated productions of TNF-α and IL-6 by human monocytes. *J Immunol* 2005;**174**:5846−55.

41. Guo X, Rao J, Yan T, Zhang B, Yang W, Sun W, et al. Feleucin-K3 analogue with an alpha-(4-pentenyl)-Ala substitution at the key site has more potent antimicrobial and antibiofilm activities *in vitro* and *in vivo*. *ACS Infect Dis* 2021;**7**:64−78.
42. Guo X, Yan T, Rao J, Yue X, Pei X, Deng J, et al. Potent antimicrobial and antibiofilm activities of Feleucin-K3 analogs modified by alpha-(4-pentenyl)-Ala against multidrug-resistant bacteria. *Biomolecules* 2021;**11**:761.
43. Wang Z, Li Q, Li J, Shang L, Li J, Chou S, et al. pH-Responsive antimicrobial peptide with selective killing activity for bacterial abscess therapy. *J Med Chem* 2022;**65**:5355−73.
44. Kremsmayr T, Aljnabi A, Blanco-Canosa JB, Tran HNT, Emidio NB, Muttenthaler M. On the utility of chemical strategies to improve peptide gut stability. *J Med Chem* 2022;**65**:6191−206.
45. Cannito S, Novo E, di Bonzo LV, Busletta C, Colombatto S, Parola M. Epithelial-mesenchymal transition: from molecular mechanisms, redox regulation to implications in human health and disease. *Antioxid Redox Signal* 2010;**12**:1383−430.
46. Liu W, Zabirnyk O, Wang H, Shiao YH, Nickerson ML, Khalil S, et al. miR-23b targets proline oxidase, a novel tumor suppressor protein in renal cancer. *Oncogene* 2010;**29**:4914−24.
47. Gao K, Wang T, Qiao Y, Cui B. miR-23b-5p promotes the chemosensitivity of temozolomide *via* negatively regulating TLR4 in glioma. *Acta Biochim Biophys Sin* 2021;**53**:979−87.
48. Zhang ZQ, Song YL, Chen ZH, Shen Y, Bai CX. Deletion of aquaporin 5 aggravates acute lung injury induced by *Pseudomonas aeruginosa*. *J Trauma* 2011;**71**:1305−11.
49. Hasan B, Li FS, Siyit A, Tuyghun E, Luo JH, Upur H, et al. Expression of aquaporins in the lungs of mice with acute injury caused by LPS treatment. *Respir Physiol Neurobiol* 2014;**200**:40−5.
50. Xu C, Jiang L, Zou Y, Xing J, Sun H, Zhu B, et al. Involvement of water channel aquaporin 5 in H_2S-induced pulmonary edema. *Environ Toxicol Pharmacol* 2017;**49**:202−11.
51. Sun CY, Zhao YX, Zhong W, Liu DW, Chen YZ, Qin LL, et al. The expression of aquaporins 1 and 5 in rat lung after thoracic irradiation. *J Radiat Res* 2014;**55**:683−9.
52. Lv X, Gao F, Zhang S, Zhang S, Zhou X, Ding F, et al. Maladjustment of beta-CGRP/alpha-CGRP regulation of AQP5 promotes transition of alveolar epithelial cell apoptosis to pulmonary fibrosis. *J Interferon Cytokine Res* 2020;**40**:377−88.
53. Gabazza EC, Kasper M, Ohta K, Keane M, D'Alessandro-Gabazza C, Fujimoto H, et al. Decreased expression of aquaporin-5 in bleomycin-induced lung fibrosis in the mouse. *Pathol Int* 2004;**54**:774−80.
54. Zhou X, An G, Chen J. Inhibitory effects of hydrogen sulphide on pulmonary fibrosis in smoking rats *via* attenuation of oxidative stress and inflammation. *J Cell Mol Med* 2014;**18**:1098−103.
55. Tan ZX, Chen YH, Xu S, Qin HY, Zhang C, Zhao H, et al. Calcitriol inhibits bleomycin-induced early pulmonary inflammatory response and epithelial-mesenchymal transition in mice. *Toxicol Lett* 2016;**240**:161−71.
56. Zhang ZD, Yang YJ, Liu XW, Qin Z, Li SH, Li JY. Aspirin eugenol ester ameliorates paraquat-induced oxidative damage through ROS/p38-MAPK-mediated mitochondrial apoptosis pathway. *Toxicology* 2021;**453**:152721.
57. Wang Y, Li X, An G, Zhu Z, Liang D, Lian X, et al. SB203580 inhibits epithelial-mesenchymal transition and pulmonary fibrosis in a rat silicosis model. *Toxicol Lett* 2016;**259**:28−34.
58. Nagaraja SS, Nagarajan D. Radiation-induced pulmonary epithelial-mesenchymal transition: a review on targeting molecular pathways and mediators. *Curr Drug Targets* 2018;**19**:1191−204.